The compressible Coanda wall jet—an experimental study of jet structure and breakaway

D. G. Gregory-Smith* and A. R. Gilchrist†

An underexpanded jet issuing from a convergent slot and blowing over a surface of convex streamwise curvature was studied experimentally. The jet was confined between side walls, with the slot aspect ratio varying between 40 and 6, but tests showed that in the area of interest close to the slot the flow was effectively two-dimensional. The ratio of slot width to the radius of curvature of the downstream surface varied between 0.05 and 0.33. The main techniques used were Schlieren and shadowgraph to show the jet structure, and surface flow visualization which revealed areas of separation and reattachment. Surface static pressures were also measured on the curved surface. The curved jet proved to have a shock cell structure similar to that of a plane jet. However, the cell structure disappeared more rapidly as the outer shear layer grew more quickly due to the destabilizing effect of the curvature on the turbulence in the shear layer. Even at modest upstream jet pressures, a separated region on the Coanda surface became evident. This region was characterized by a stagnant constant pressure part followed by a region of strongly reversed flow before reattachment took place. The separation was caused by the compression at the end of the first shock cell, with reattachment taking place where expansion in the second cell started. The separated region grew rapidly as the upstream pressure was increased, until, finally, reattachment failed to occur and the jet suddenly broke away from the surface. This work is related to studies of the Coanda flare, where the jet is axisymmetric. The high level of turbulence causes rapid entrainment of air and so gives us clean combustion. However there should be more general application to devices that use the Coanda effect, varying from fluidic devices to blown jet flaps on wings.

Keywords: *Coanda effect, compressible wall jet, underexpanded jet, two-dimensional flow, turbulence, shock cells*

Introduction

The Coanada effect is used to describe the phenomenon whereby a jet blown over a surface of convex streamwise curvature adheres to the surface. The effect has been studied widely since the last century, and three important features may be identified[1,2]:

(1) an inviscid effect whereby a curved flow will remain attached to a curved surface;
(2) a viscous effect whereby a jet placed close to a curved surface will tend to be drawn towards the surface because of the low pressure created by the jet entrainment;
(3) the higher entrainment by a curved wall jet compared with a plane wall jet; this is caused by the destabilizing effect of the curvature on the turbulence in the outer part of the jet.

The Coanda effect has found wide application: from small fluidic devices to re-energizing boundary layers on aircraft wings and jet flap devices. The particular application which prompted this work is the design of Coanda flares (see Fig 1). High pressure combustible gas emerges from a slot at the base at an axisymmetric tulip-shaped body. The jet adheres to the surface, and the high entrainment rate of ambient air into the curved jet leads to good premixing and efficient combustion with low radiation and low smoke pollution. British Petroleum plc have developed these flares as described by Wilkins *et al*[3]. Noise aspects have been studied at Exeter University[4], while at Durham University the aerodynamics of the curved jet has been investigated. Morrison and Gregory-Smith[5] have reported a calculation method for the development of the low speed jet, and have compared its predictions with Morrison's[6] experimental results.

In practice the gas supply pressure is above that required for choked flow, and the issuing jet is underexpanded. If the supply pressure is raised sufficiently, the jet can break away from the surface, forming a free jet. The main aim of this work was to study the structure of the underexpanded curved wall jet, and the mechanism of breakaway.

Compressible and curved wall jets

Close to the nozzle, the wall jet consists of three parts: a thin boundary layer on the surface, a potential core, and a growing outer shear layer. If the jet is underexpanded, the potential core has a shock-cell type of structure, as is observed for free jets. The mixing with ambient air causes the shear layer to grow, so that the shock cell structure becomes indistinct after a few cells. The potential core disappears, and further downstream the velocity profile becomes fully developed as for a low speed wall jet. As is shown below, the mechanism of breakaway occurs within the first one or two shock cells, and the shock cell structure is very important.

The structure of underexpanded free jets has been studied widely. For instance, Love *et al*[7] describe a detailed study of circular underexpanded jets issuing from convergent or convergent–divergent nozzles. Benson and Poole[8] investigated the structure of a two-dimensional jet over a wide range of pressure ratios. Ignoring the presence of the boundary layer, a plane wall jet may be thought of as half a free jet, with the surface forming the axis of symmetry. Benson and Poole found that at upstream pressures just above that required for choking, the

* School of Engineering and Applied Science, University of Durham, Science Laboratories, South Road, Durham, DH1 3LE, UK
† Formerly of the School of Engineering and Applied Science, University of Durham
Manuscript received 9 July 1986 and accepted for publication on 19 December 1986

0142-727X/87/020156-09$3.00

structure is as shown in Fig 2(a). The Mach waves from the initial Prandtl–Meyer expansion at A are 'reflected' at the jet axis (B) and then reflected off the free surface (C) as compression waves. The compression waves are reflected at D and coalesce to form an oblique shock at F. As the upstream pressure is increased, the coalescing of the compression waves occurs at E before the jet axis, the resulting shock wave being reflected at the jet axis (Fig 2(b)). At still higher upstream pressures, the oblique shock becomes highly curved and leads to the formation of a normal shock wave across the jet axis (Fig 2(c)): in a round jet this normal shock is known as the Mach disk.

Very little work has been published on underexpanded wall jets over plane or curved surfaces. However low speed wall jets have been studied extensively: for instance Refs 9–11 for two-dimensional jets, and Refs 6, 12 and 13 for axisymmetric jets. Some studies have been done on the deflection of compressible jets by adjacent surfaces. Roderick[14] investigated deflection caused by a surface that consisted of a short plane section fixed tangentially at a 90° circular arc. The plane section was set at an angle to the initial jet axis, varying between 0° and 25°. Korbacher[15] measured the static pressure distribution over a surface similar to that of Roderick. Bradbury and Wood[16] investigated the deflection of a thick jet ($b/a=0.5$) over a deflection surface that consisted of a circular drum with a plane flap attached tangentially to it. For above choking upstream pressures small deflections of the jet occurred before breakaway. Gregory-Smith and Robinson[17] and unpublished work from British Petroluem showed that as the ratio of slot width to streamwise radius of curvature of the surface decreased, the upstream pressure required for breakaway increased. Also there was a hysteresis effect in that after breakaway the pressure had to be reduced considerably before reattachment of the jet took place.

Experimental apparatus

Although the actual Coanda flare is axisymmetric, it was decided to study the flow with a two-dimensional model, ie the jet blowing over a cylindrical Coanda surface. This made much simpler the use of optical flow visualization techniques: interferometry, Schlieren, and shadowgraph.

The model, shown in Fig 3, had a 30 mm radius of curvature for the Coanda surface, which then became a plane surface after 100° from the slot exit. The dimensions of the channel upstream of the slot were chosen to model approximately an axisymmetric flare. Two nozzle lip profiles were used, the difference being in the thickness, so that for nozzle A the slot exit was on a radial line from the centre of curvature of the downstream surface, while for nozzle B there was a 1.5 mm flat part between slot exit and the start of the curvature. By sliding the upper section relative to the nozzle lip, the slot width was varied between 1.5 mm and 10 mm, with most tests being done at 4 mm. The air supply restricted the breadth of the model to 60 mm, so the slot aspect ratio varied between 40 and 6. Care was taken to ensure uniformity of slot width; the maximum measured variation was 0.01 mm, ie 0.25% for a 4 mm width.

The Coanda surface contained 0.75 mm diameter surface pressure tappings at every 5° over the first 40° and every 10° thereafter. The tappings were staggered across the central

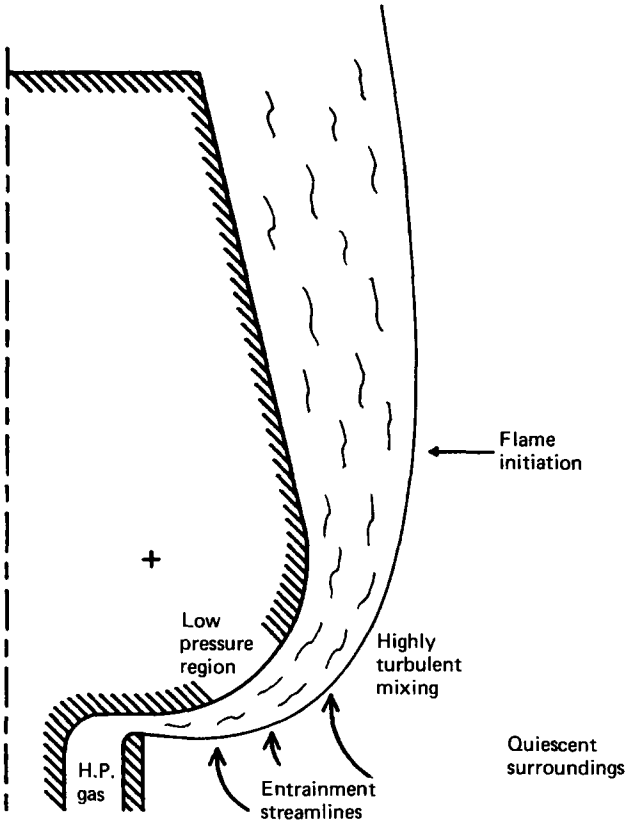

Figure 1 Principles of Coanda flare

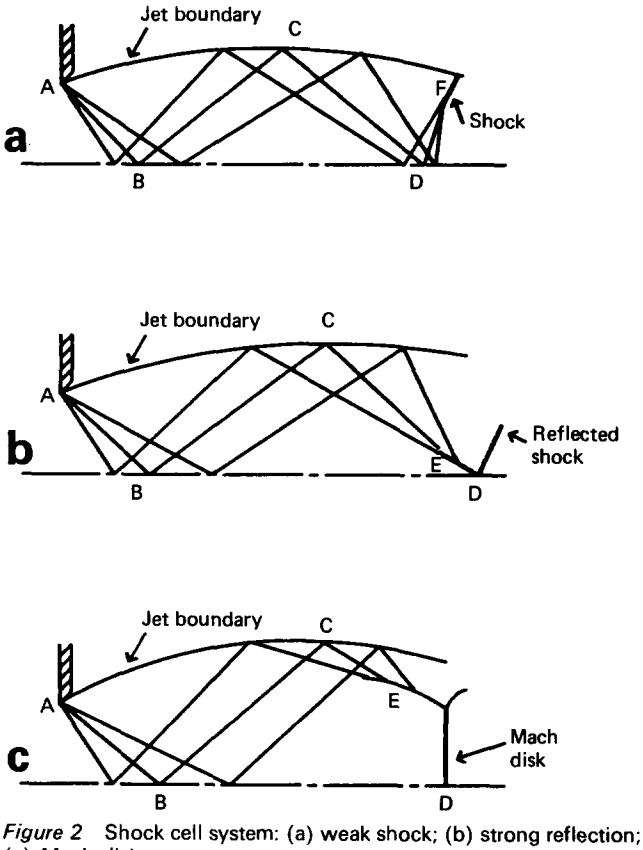

Figure 2 Shock cell system: (a) weak shock; (b) strong reflection; (c) Mach disk

Notation

- a Downstream streamwise radius of curvature
- b Slot width
- C_d Discharge coefficient
- p_a Downstream (atmospheric) pressure
- p_0 Upstream stagnation pressure
- p_s Surface static pressure
- λ Wavelength of light

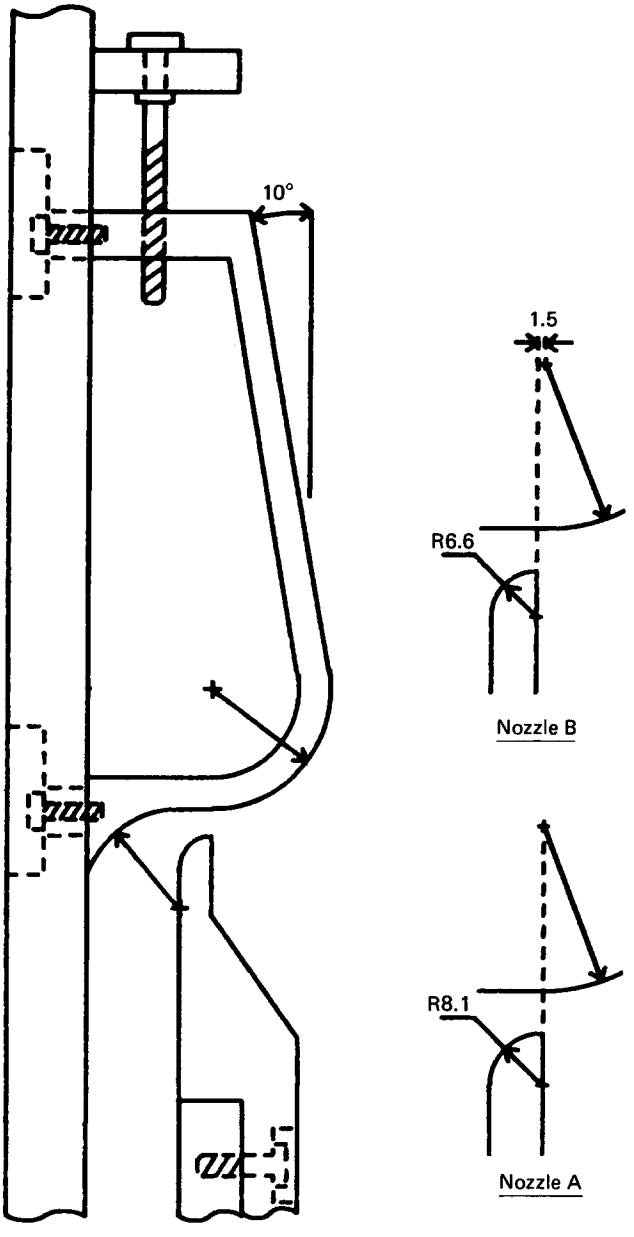

Figure 3 Coanda model (dimensions: mm)

30 mm of the breadth of the surface. The apparatus was placed between side walls which contained 100 mm diameter windows placed to give the maximum view of the developing jet. For the optical measurements, the windows contained 25 mm thick glass flats ($\lambda/20$), but these were replaced by Perspex for some surface flow visualization studies.

The apparatus was supplied from a 30 bar air main via a pressure-regulating reduced valve, filters and an orifice flow meter. Once set, the pressure at the apparatus drifted by less than 0.02 bar over a long trial period. Upstream pressure was measured with a calibrated Budenberg gauge, and the pressure tappings were connected to mercury or water inclined manometers.

The optical apparatus is described in detail by Gilchrist[18], but in essence consisted of a Z-configuration as shown in Fig 4, which shows the set-up for interferometry. A helium–neon laser beam was split at B1, the reference beam passing straight on, and the measuring beam being expanded by the lens L1 and the parabolic mirror M1. After contraction from M2 and L2, the measuring beam was recombined with the reference beam at B2, before being projected onto a screen or photographic film.

For Schlieren and shadowgraph pictures, it was found preferable to replace the laser by a xenon spark source, which could give either a spark picture from one high intensity spark or a continuous picture from a series of low intensity sparks. With the reference beam obscured, shadowgraph pictures could be obtained, and with the addition of knife edge at the focus of M2 before the lens L2, Schlieren pictures could be obtained. The advantage of the arrangement was that no alteration of the optical components (apart from the light source) was required to change from one technique to another.

Preliminary tests

In order to check the two-dimensionality of the flow, several traverses were made across the jet, using a small pitot tube with slot widths of 2 mm and 4 mm. These were made at angles of 0°, 20° and 40° around the curved Coanda surface, and at various distances from the surface. The results showed uniform flow across the slot breadth except for the influence of the side walls. At an angle of 40°, for the 4 mm slot width, the influence extended for a maximum of 20% of the breadth, leaving the central 60% of the flow unaffected. For the 2 mm slot width the maximum extent was 12% of the breadth.

Although the boundary layer on the side walls is initially very thin, its interaction with the curved flow causes strong secondary flows. The secondary flows were observed using a surface flow visualization technique. A pink 'Dayglo' pigment was mixed with a silicone fluid and painted on the Coanda surface and side walls, which were covered with a cellophane film. The pigment fluoresced under ultraviolet light, allowing good photographs to be taken. The technique was also used to investigate the flow separation bubble on the Coanda surface (see below). Fig 5 shows a typical view of the curved surface, taken while the rig was running; the extent of the secondary flows near the side walls can be seen, with horizontal separation lines unaffected over the central part of the flow.

While it appears that flow far downstream of the slot was influenced by the secondary flows, it was concluded that for the purposes of this study, which was concerned with the flow near the slot, the results would not be significantly affected.

The discharge coefficient of the nozzles was measured, primarily to enable the mass flow to be determined from the upstream static pressure, thus allowing calculation of the upstream stagnation pressure. The results for nozzle A are shown in Fig 6, plotted against the ratio of atmospheric pressure to upstream stagnation pressure, p_a/p_0. The results were corrected for a leakage estimate obtained with a rubber sheet clamped between the curved surface and the nozzle lip. The maximum correction was around 1% for the 2 mm slot. The estimated maximum error in discharge coefficient is 1.6% for the 2 mm slot, reducing to 1.1% for the 8 mm slot. The results in Fig 6 show that the largest slot width has the lowest discharge coefficient, because of the greater nonuniformity of the flow through the slot caused by the upstream curvature of the nozzle lip. The coefficient rises as the inlet pressure rises, as found by other workers[19,20]. However, the coefficient for the 2 mm slot rises above unity, exceeding it by a maximum of 1.8%, which is more than the estimated error. This is possibly due to distortion

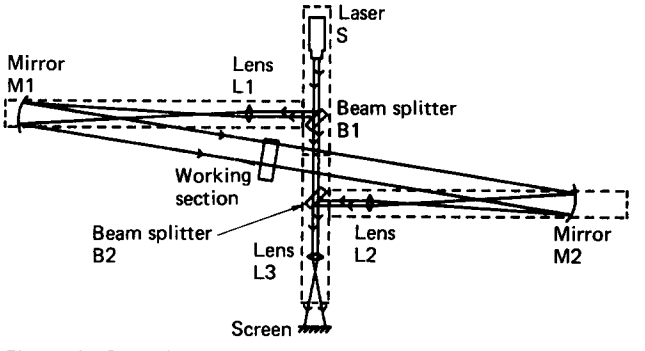

Figure 4 Optical system

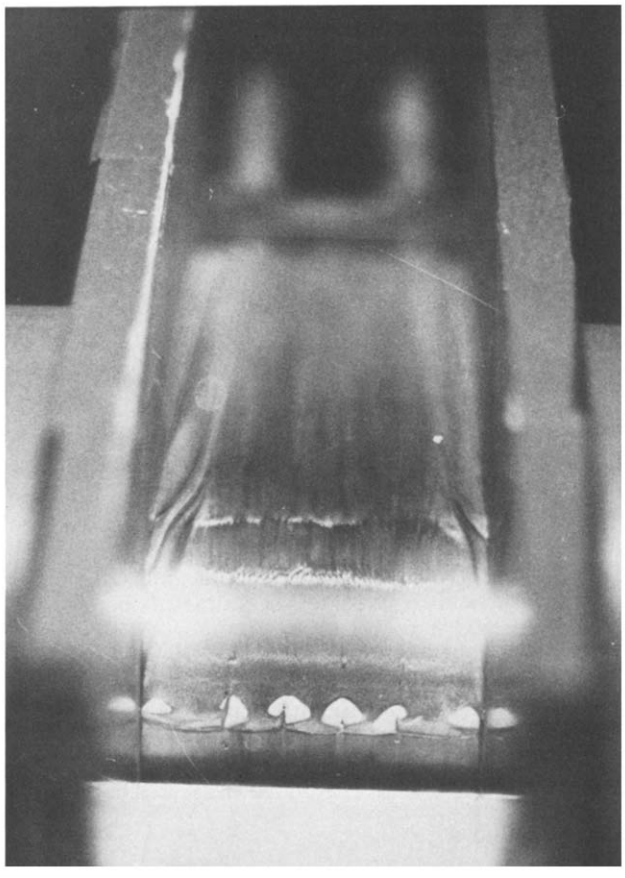

Figure 5 Coanda flow visualization, slot=4 mm

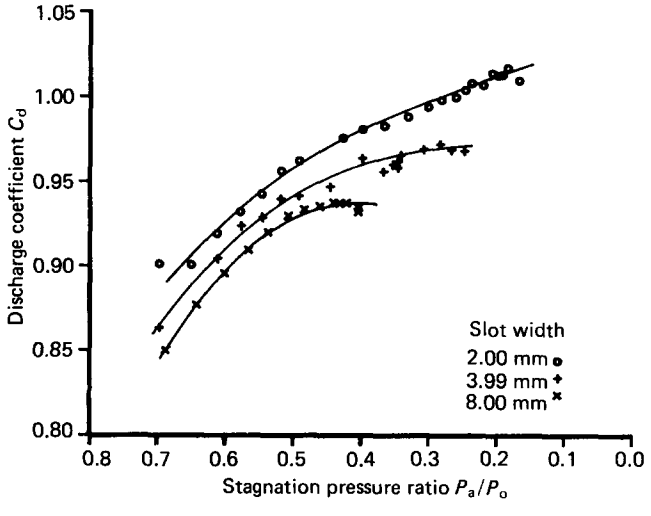

Figure 6 Coefficient of discharge, Nozzle A

at the higher inlet pressures or to the leakage rate being underestimated, since the limit of leakage measurements was a pressure ratio of 0.28.

Jet breakaway and reattachment

The breakaway stagnation pressure ratio was defined as the ratio of atmospheric pressure to upstream stagnation pressure at which the jet 'flipped' from the curved Coanda surface to a horizontal free jet. As the stagnation pressure was reduced after breakaway, the jet was deflected towards the curved surface by up to 10°, before it 'flipped' back onto the Coanda surface. This defined the reattachment stagnation pressure ratio. For each slot width, up to eight readings of breakaway and reattachment were taken and averaged.

The results are shown in Fig 7 for nozzle A; the results for nozzle B were almost identical. As previous work had shown, the breakway and reattachment occurred at higher upstream pressures as the slot width was reduced. The hysteresis between breakaway and reattachment increased as the slot width was reduced.

A discontinuity in the breakaway results was noticed at a slot width to downstream radius ratio (b/a) of 0.14, and so a retest was carried out. There were small but significant differences from the original test, and these do not appear to be attributable to measurement error. However, the region between reattachment and breakaway is a bistable region, and it is possible that some undetected external influence was affecting the stability.

Surface static pressures

The surface static pressures were measured for a range of upstream pressures using nozzle A. The results for unchoked flow are described by Gilchrist[18], and only those for choked flow are presented here. Fig 8(a) shows the surface pressure plotted against the angle for the 4 mm (nominal) slot. At the upstream pressure just above choking ($p_a/p_0=0.513$), the surface pressure was subatmospheric everywhere on account of the curvature of the flow, but with a slight waviness near the slot caused by one or two small shock cells. The rise towards 100° was due to the change from a curved to a flat surface at 100°. As the upstream pressure was increased, the amplitude and period of the waves was increased, with the shock cells becoming stronger and longer. In general, the surface pressure first fell rapidly as the Prandtl–Meyer expansion waves reached the surface, and then it rose as the compression waves from the free edge of the jet arrived. The process was repeated in subsequent cells, but the mixing with ambient air caused a reduction in their strength.

However, as the upstream pressure was further increased towards breakaway (Fig 8(b)), the minimum static pressure

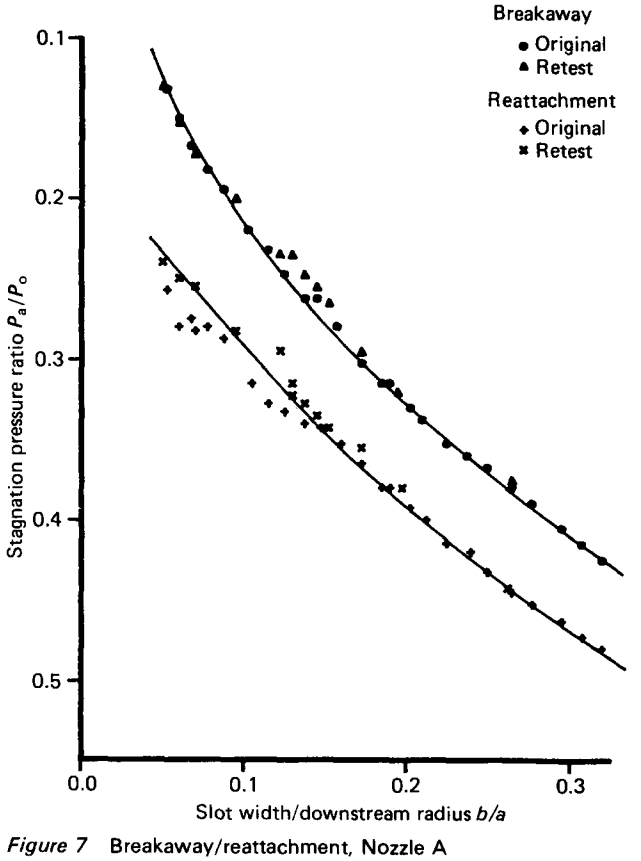

Figure 7 Breakaway/reattachment, Nozzle A

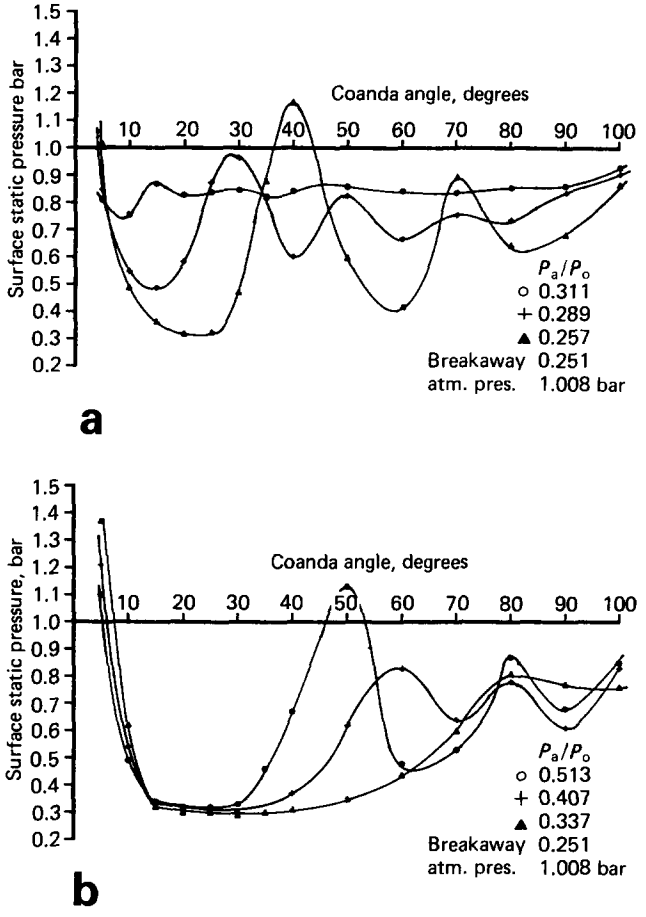

Figure 8 Surface static pressures, slot=4.15 mm: (a) higher pressure ratios; (b) lower pressure ratios

became nearly constant, and extended over an increasing angle. Also, the first peak in pressure began to decrease in amplitude. Just before breakaway, the constant minimum pressure extended from approximately 15° to 45° around the surface, and the peak of the first pressure recovery occurred at 80°.

The results of measurements with 2 mm, 6 mm and 8 mm slot widths were similar to the 4 mm results. As the slot width was increased, the length of the first shock cell increased, and the pressure recovery at the end was less. A notable feature for slot widths was that, just before breakaway, although the angular position of the start of the constant minimum pressure region increased with slot width, the start of the pressure recovery was always at approximately 45° and the first peak at approximately 80°.

Results for a 2 mm slot using nozzle B were very similar to those using nozzle A.

Surface flow visualization

As mentioned above, surface flow visualization was carried out while checking the two-dimensionality of the flow. It was also used to investigate any regions of separation or reattachment of the boundary layer on the Coanda surface. Visualization was carried out at slot widths of 2 mm, 4 mm and 8 mm. As can be seen in Fig 5, a number of bands appeared, the position of which could be recorded in relation to the surface pressure tappings, whose angular positions were known. In general this was done by visual observation while the rig was running, as the bands tended to collapse while the rig was being shut down. At high inlet pressures, regions of reverse flow between some of the bands could be observed as fluid was 'flicked' from one band to the next one downstream by the mainstream flow, the fluid then running back along the surface to the original band. In Fig 5 four bands can be seen: the first wide one, smaller ones just above and below the glare, and the fourth band situated at the start of the flat part of the surface. Six accumulations of oil can be seen within the first band: one in each corner, and the other four apparently caused by small disturbance from the static pressure tappings. It was not thought that these disturbances affected the main flow. Fluid from the accumulations was picked up by the mainstream flow and deposited on the second band, just below the glare. The fluid then flowed rapidly back to the trailing edge of the first band.

Fig 9 shows the position of the bands at varying pressures for the 4 mm slot. The shaded areas show the first three bands, the fourth being excluded. Arrows between the first two bands indicate the region of reversed flow. At inlet pressures well below breakaway with the 2 mm slot, four bands were observed, while at 8 mm only two bands could be seen (apart from the band at the start of the flat surface). However, in all cases, as the inlet pressure was raised, the bands moved downstream and disappeared until only the first two bands remained, the second band reaching approximately 70° before breakaway occurred. The start of the first band depended on slot width. Just before breakaway it was at about 10° for the 2 mm slot, increasing to about 30° for the 8 mm slot.

It thus appears that the first band was caused by a separation of the boundary layer on the Coanda surface and indicated a fairly stagnant region. Reattachment took place at the second band, with a strong region of reversed flow back to the stagnant region. The subsequent bands at the smaller slot widths were caused by less severe later separations and reattachments.

Optical results

The three optical techniques are useful for revealing different features of a compressible flow field. With interferometry used in the finite fringe mode, the shift of a fringe compared with its undisturbed position depends on the density of the flow. Thus quantitative information on density values may be obtained, and under certain conditions, eg isentropic flow, the other flow properties such as Mach number and static pressure may be deduced. However, with Schlieren and shadowgraph methods, usually only qualitative information is obtained. With the Schlieren technique the intensity of illumination depends on the gradient of density, and is thus most useful for showing regions of compression or expansion. The orientation of the knife edge determines the spatial direction for the derivative of density, and the results presented here show either vertical or horizontal gradients. Shadowgraph shows the second spatial derivative of density, and is useful for highlighting sudden changes in density such as occur at shock waves.

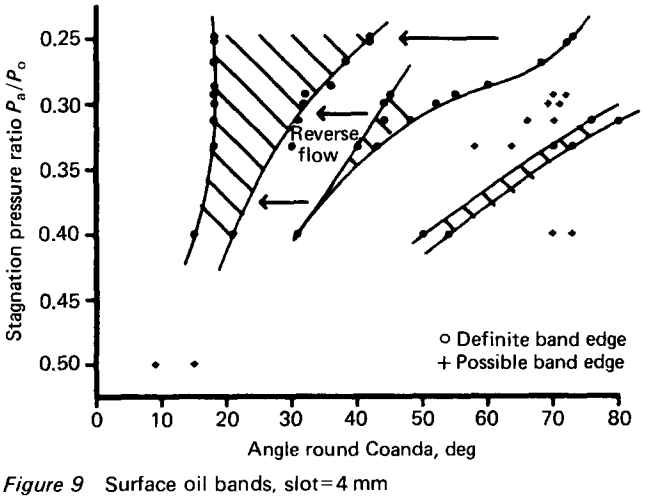

Figure 9 Surface oil bands, slot=4 mm

The interferometry gave clear pictures for inlet pressures up to choking, and useful quantitative information was obtained for the subsonic jet (see Gilchrist[18]). However, although precautions were taken against vibration, it was found impossible to obtain clear pictures at higher inlet pressures. Some development of the optical apparatus is required in order to obtain results for the underexpanded jet. However, much information was obtained from the Schlieren and shadowgraph pictures, some of which are presented here.

Fig 10 shows the shadowgraph for the 4 mm slot at a modest pressure ratio of 0.323, breakaway being at 0.240. The stagnation temperature of the inlet air was close to atmospheric temperature, and so on expansion through the nozzle, the exit temperature was well below atmospheric. Thus the jet density was higher than atmospheric, and the change is shown by the line at the edge of the jet for the first shock cell. There are several disturbances in the flow as it approaches the slot exit, the majority emanating from the lower nozzle profile. These culminate in an oblique line at the nozzle lip that reaches the downstream surface at about 8°. These disturbances indicate that the acceleration inside the nozzle is not smooth and that a weak oblique shock exists at exit. Some faint reflections of the waves from the nozzle lip can be seen, but a clearer weak shock can be seen coming from the curved surface at about 17°. Just downstream of the weak shock there is a dark line which appears to indicate a small separation of the flow from the curved surface. At about 35°, where the flow appears to reattach, a stronger oblique shock is seen. The shock is bent near the jet edge, with a second shock returning to the surface at about 43°. An additional disturbance can be seen at about 75° around the surface.

Figs 11(a) and 11(b) show the Schlieren pictures for the same conditions as Fig 10. Fig 11(a) shows vertical density gradients, a dark region indicating an increase in density from top to bottom. Fig 11(b) shows horizontal gradients, a dark region indicating an increase in density from left to right. The region within the nozzle is light, indicating an expansion of the flow,

Figure 10 Shadowgraph, $p_a/p_0=0.323$, slow=4 mm

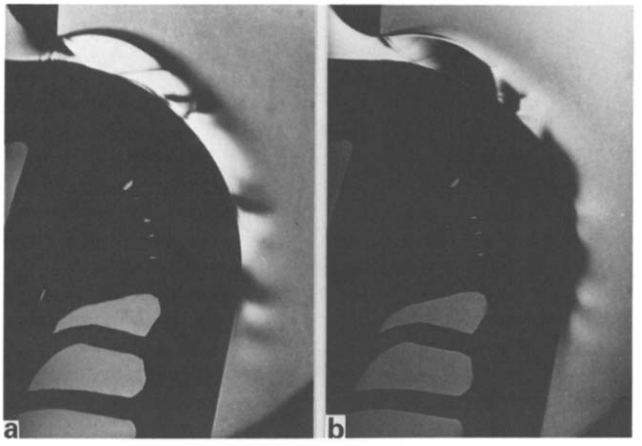

Figure 11 Schlieren, $p_a/p_0=0.323$, slot=4 mm: (a) vertical density gradients; (b) horizontal density gradients

but Fig 11(a) shows that, across the exit, conditions are not uniform, with a lower density at the nozzle lip. This is due to the lower pressure on the convex surface of the nozzle profile. As with the shadowgraph, some disturbances inside the nozzle are visible. The density continues to fall through the Prandtl–Meyer expansion fan centred at the nozzle lip. The bowed edge of the jet is more clearly seen than with the shadowgraph. The other features observed with the shadowgraph are also seen, in particular the separation with the weak shock at its front, and the lower shocks at its rear. In addition, repeated expansion and contraction through at least two further shock cells may be seen.

The effect of increasing the upstream pressure towards breakaway may be seen in Fig 12, which is the Schlieren picture showing horizontal density gradients at a pressure ratio of 0.241. The first cell is longer and wider at its maximum extent, but the most noticeable feature is the very large separated region. A stronger shock wave is seen from the front of the separated region, which is reflected from the free surface as a series of expansion waves, causing a narrowing of the separated region. Presumably, the falling pressure in the expansion waves causes reattachment of the flow, but with a thick boundary layer formed. Fig 13 shows the spark Schlieren for nearly the same conditions as Fig 12. After the first shock cell, the growth of the shear layer causes a rapid encroachment of turbulence into the potential core. The latter part of the separated region also appears fairly turbulent.

Fig 14 shows the jet from the 4 mm slot broken away from the Coanda surface, leaving it at about 10°. The jet resembles a free jet by the end of the first shock cell, with subsequent alternating regions of expansion and compression. Within the first shock cell the compression starts earlier at the surface, with the shock wave which turns the flow away from the surface.

The results with a 2 mm slot and 8 mm slot show a similar structure to that for the jet from the 4 mm slot, but with the first shock cell extending further around the surface as the slot width is increased. Thus, the start of the separation is also further downstream with the wider slots. The encroachment of turbulence into the first shock cell for the 8 mm slot is very small compared with the slot width. However, the core quickly disappears after the third shock cell, as with the jets from the 2 mm and 4 mm slots.

Discussion

In their study of an incompressible self-preserving wall jet, Guitton and Newman[21] identified two main causes for the departure from two-dimensionality. The first relates to conditions in the plenum chamber and in particular at the nozzle lip, and the second results from the secondary flows on the side walls. For small ratios of slot width to downstream radius of curvature, giving a fully developed jet, any disturbance

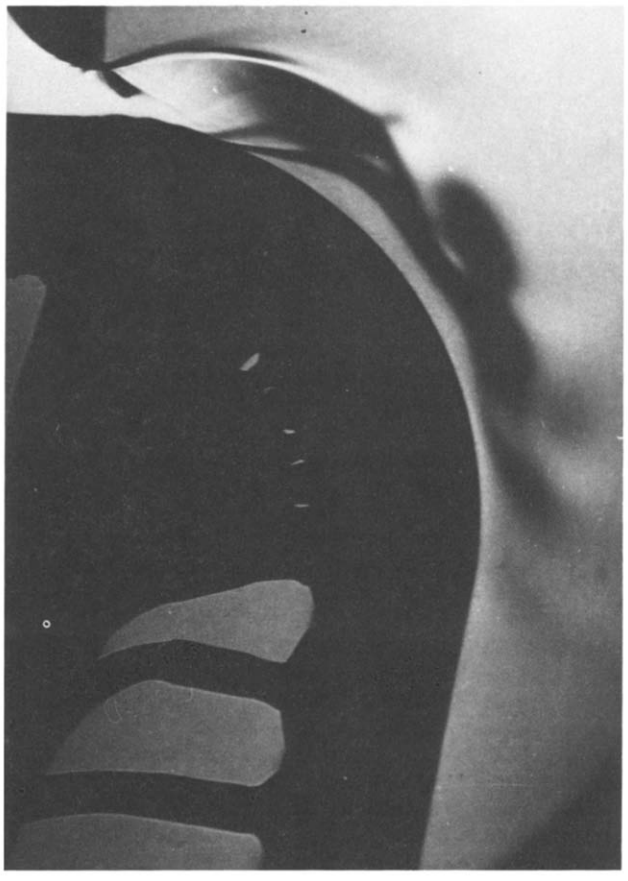

Figure 12 Schlieren, $p_a/p_0=0.241$, slot=4 mm, horizontal density gradients

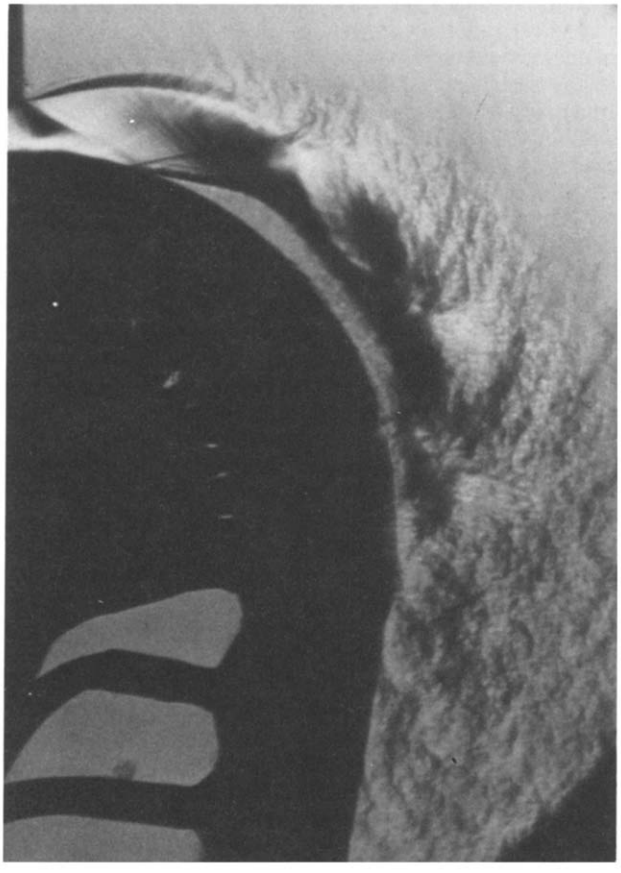

Figure 13 Spark Schlieren, $p_a/p_0=0.244$, slot=4 mm, horizontal density gradients

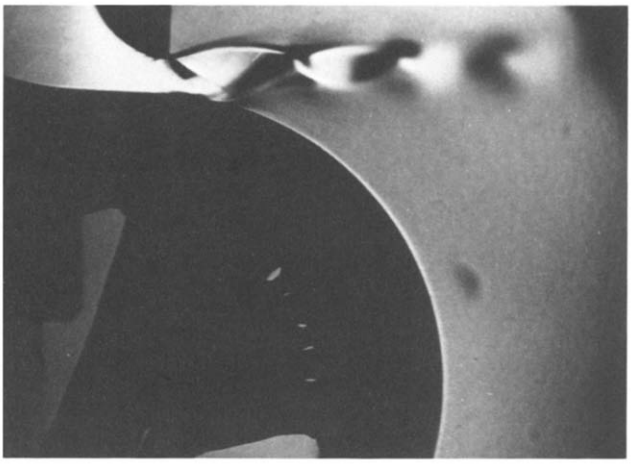

Figure 14 Schlieren, breakaway, slot=4 mm, horizontal density gradients

caused by slot width nonuniformity tends to be amplified downstream. For these tests, great care was taken in manufacture to ensure uniform slot width, and the preliminary traverses showed that conditions were uniform away from the influence of the secondary flows. In addition, the ratio of slot width to radius of curvature was relatively large, and as regards breakaway, the region of interest is confined to the first shock cell and the start of the second, where the potential core is still very significant. Thus, although the secondary flows penetrated the breadth of jet, typically 20% from both walls, reasonable confidence can be taken that the overall results were not significantly affected by non-two-dimensional effects, in spite of the fairly low slot aspect ratios.

The existence of a separation bubble at upstream pressures well below that required for breakaway is shown by the Schlieren and shadowgraph photographs, by the static pressure distributions and by the surface flow visualizations. Moreover the latter experiments revealed a region of reversed flow on the surface within the separation bubble. From all the above experiments it was possible to estimate angular positions for the initial separation, the end of the constant pressure region, and the reattachment point. Fig 15 shows these results for the 4 mm slot width. From the static pressure distributions, the angle of initial separation was taken as the angle at which the static pressure became constant, the end of the constant pressure region was estimated from the start of the pressure rise, and the angle of reattachment estimated from the angle at the peak of the pressure rise.

As the pressure ratio is reduced (upstream pressure increased), the angle of initial separation first increases and then becomes constant as breakaway is approached. Also, the extent of the constant pressure region is increased, as is the region of reversed flow. The angle of reattachment increases with reducing pressure ratio, the rate of increase becoming greater as breakaway is approached, reaching an angle of about 80°. Fig 15 shows that the determination of the positions of the regions is consistent between the various methods of their measurement. In particular, the region of constant static pressure corresponds to the stationary separated region shown by the flow visualization, and the pressure rise corresponds to the region of reversed flow.

It is clear that the structure of the compressible jet core and the separated region strongly interact. It is the compression waves produced by the reflection from the free surface of the expansion fan that cause the initial separation, but the separation itself causes a shock wave, modifying the first shock cell and the subsequent pressure rise. This modification to the cell structure at pressures near breakaway is so large that the initial separation stabilizes well upstream of the compression caused by the reflection from the free surface of the Prandtl–Meyer expansion waves. The fact that the angle of initial

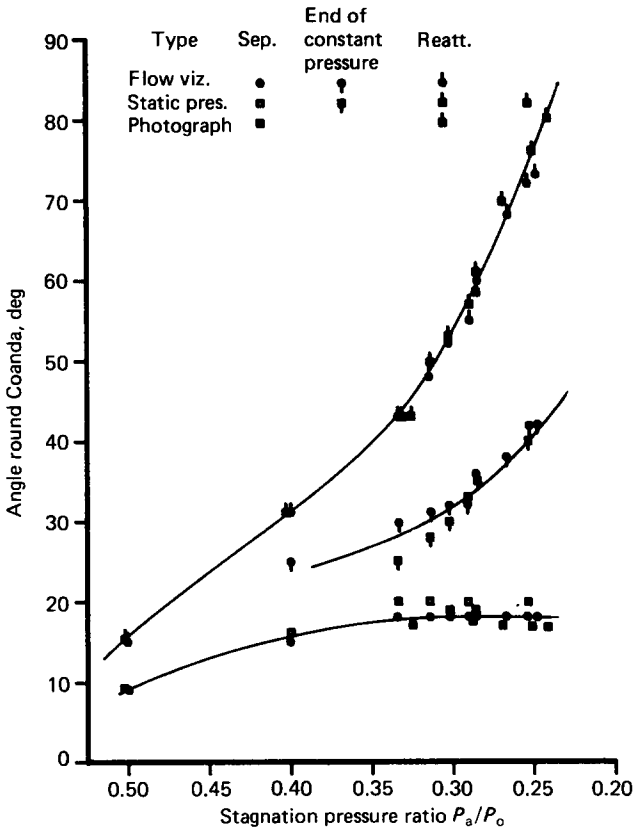

Figure 15 Correlation of separation bubble, slot=4 mm

separation becomes constant, as does the pressure in the separated region, shows this modification, since without it one would expect that the value of minimum pressure would decrease and that its position would move further around the surface as the inlet pressure was raised.

The mechanism of breakaway appears to be that the separated region grows rapidly as breakaway is approached, until a critical point is reached when reattachment fails to take place. The furthest position for reattachment does not change much with slot width. Results corresponding to those of Fig 15 show that the maximum extent for the 2 mm slot was 70°, for the 4 mm slot 80°, and for the 8 mm slot 83°. This variation is not great over a fourfold change in slot width and when compared with the scatter in results. It is possible that the failure to reattach is affected by the presence of the downstream flat causing a pressure rise; Fig 8 shows the pressure rising from 90° onwards. If so, it would be expected that curved Coanda surfaces which turned the flow through a smaller angle would break away at a lower upstream pressure, and that the breakaway for a larger turning angle would be at a higher pressure. Some unpublished work from British Petroleum reports an investigation of jet flow over cylindrical arcs of included angles from 60° to 180°. Initially, the breakaway pressure rose with increasing angle, but then levelled off at about 120°. Thus, at 100° the flat in these experiments may be having a slight effect. Tests on axisymmetric flares have shown a much higher pressure required for breakaway for the same ratio of slot width to downstream radius of curvature. This is because the radial outflow effectively thins out the jet.

After breakaway, the inlet pressure has to be reduced considerably before the jet reattaches. This means the shock cell structure becomes smaller, until the entrainment of the free jet becomes large enough, compared with the jet momentum, to suck the jet back onto the surface. For the 4 mm slot, reattachment takes place at a pressure ratio close to that at which the pictures in Figs 10 and 11 were taken. The shock cell structure and the separation bubble are quite small compared with those near breakaway (Fig 12), suggesting that the conditions close to the slot determine reattachment. The British Petroleum results referred to above show no change in reattachment pressure with the angle of arc of the curved surface.

The two slightly different upstream nozzle profiles give the same results for breakaway and reattachment. This is to be expected in view of the mechanisms described above. Changing the profile had a very small effect on the shock cell structure, and so the conditions for breakaway and reattachment were unaltered.

Conclusions

A two-dimensional model, based on an axisymmetric Coanda flare, was used to investigate the behaviour of the curved wall jet at high jet pressures. Schlieren and shadowgraph optical techniques along with surface flow visualization and pressure distribution measurements helped to reveal the structure of the jet and the mechanism of breakaway. Preliminary tests showed that the flow in the area of interest was primarily two-dimensional, and that the nozzle coefficient of discharge rose with upstream pressure in a way similar to that observed by other workers.

The jet conditions studied were for an underexpanded jet, whose structure is similar to that of a plane jet. There is a shock cell structure, with an expansion fan centred on the nozzle lip giving rise to waves which are later reflected from the free surface as compression waves. The shear layer within the ambient air does not affect the first shock cell very much. However, the curvature causes a rapid encroachment of turbulence into the shock cell structure, so that it disappears after two or three shock cells. This dissipation of the potential core is much more rapid than with a free jet (see Fig 14, where four cells can be seen in the broken-away jet).

The compression waves at the end of the first shock cell cause a separation of the boundary layer on the curved Coanda surface. At low pressures the separated region is quite small, but as the inlet pressure is raised, it grows both in thickness and extent around the surface. Its presence modifies the shock cell structure, with the point of separation initiating a shock wave which gets stronger as the pressure is increased. The separated region contains a stagnant constant pressure region followed by a region of strongly reversed flow as the pressure rises. Reattachment takes place with the expansion at the start of the second shock cell. There is some evidence of subsequent separation and reattachment.

As the pressure is raised towards breakaway, the reattachment point moves rapidly downstream, until, at about 80° around the surface, reattachment no longer takes place. The jet 'flips' away from the Coanda surface and forms a free jet, very similar to a plane two-dimensional free jet. The upstream pressure required for breakaway is lower for a larger ratio of slot width to radius of curvature of the Coanda surface. However, the maximum extent of the reattachment before breakaway increased only slightly as the slot width increased. Although the downstream flat at 100° may be having a small effect on breakaway, the primary cause is the shock cell structure close to the slot. Once broken away, the jet pressure has to be reduced considerably to allow the shock cell structure to become weak enough for the jet to reattach.

In order to predict breakaway, which is important for the designer, the calculation of the complete jet is required, including the shear layer and the separated region. This is a very complex task, but the results here suggest that some indication of breakaway conditions may be made by calculating the first shock cell structure. A subsequent paper by the authors[22] attempts to do this.

Although these results are helpful in understanding the structure of the two-dimensional curved wall jet, for the Coanda flare application, the axisymmetric wall jet needs to be studied. The shock cell structure and the basic mechanism of breakaway

are likely to be similar, but the thinning of the jet due to the radial outflow will alter the quantitative values. Further work could also be done on methods used to delay breakaway, such as steps on the Coanda surface at the nozzle exit. These studies should enable improvements in Coanda flare design and the application of curved jets to other situations.

Acknowledgement

The authors gratefully acknowledge the support of British Petroleum plc and the SERC for this work.

References

1 Willie, R. and Fernholz, H. Report of the first European Mechanics Colloquium on the Coanda effect. *J. Fluid Mech.*, 1965, **23**,801
2 Bradshaw, P. Effects of streamline curvature on turbulent flows, AGARDograph 169, 1973
3 Wilkins, J., Withridge, R. E., Desty, D. H., Mason, J. T. M. and Newby, N. The design and development and performance of Indair and Mardair flares. Offshore Technology Conference, 1977, Houston, Paper No 2822
4 Carpenter, P. W. and Green, P. N. Noise sources in external Coanda-type gas flares. 8th Aeroacoustics Conference, Atlanta, 1983, Paper No A1AA-83-0758
5 Morrison, J. F. and Gregory-Smith, D. G. Calculation of an axisymmetric turbulent wall jet over a surface of convex curvature. *Int. J. Heat and Fluid Flow*, 1984, **5**(3), 139–148
6 Morrison, J. F. A study of the axisymmetric wall jet with streamline curvature and its application to the Coanda flare, PhD Thesis, Durham University, 1982
7 Love, E. S., Grigsby, C. E., Lee, L. P. and Woodling, M. J. Experimental and theoretical studies of axisymmetric free jets, NASA Tech. Rep. R-6, 1959
8 Benson, R. S. and Poole, D. E. Compressible flow through a two-dimensional slit. *Int. J. Mech. Sci.*, 1965, **7**, 315
9 Newman, B. G. The deflection of plane jets by adjacent boundaries—Coanda effect. In *Boundary Layer Theory and Flow Control*, ed. Zachmann, G. V., Pergamon Press, 1961, 232
10 Wilson, D. J. and Goldstein, R. J. Turbulent wall jets with cylindrical streamwise surface curvature. *ASME J. Fluids Eng.*, 1976, **98**, 550
11 Launder, B. E. and Rodi, W. The turbulent wall jet—measurement and modelling. *Ann. Rev. Fluid Mech.*, 1983, **15**, 429
12 Bakke, P. An experimental investigation of a wall jet. *J. Fluid Mech.*, 1957, **2**, 467
13 Sharma, R. N. Experimental investigation of conical wall jets. *AIAA*, 1981, **19**, 28
14 Roderick, W. E. B. Use of the Coanda effect for the deflection of jet sheets over smoothly curved surfaces, Pt II—some tests with supersonic over and under expanded jet sheets. *U.T.I.A.*, 1961, T.N. No. 51
15 Korbacher, G. K. The Coanda effect at deflection surfaces detached from the jet nozzle. *Can. Aero. Sp. J.*, 1962, **8**, 1
16 Bradbury, L. J. S. and Wood, M. N. An exploratory investigation into the deflection of thick jets by the Coanda effect, RAE, 1965, Tech. Rep. 65235
17 Gregory-Smith, D. G. and Robinson, C. T. The discharge from a thin slot over a surface of convex curvature. *Int. J. Mech. Sci.*, 1982, **24**, 329
18 Gilchrist, A. R. The development and breakaway of a compressible air jet with streamline curvature and its application to the Coanda Flare, PhD Thesis, Durham University, 1985
19 Benson, R. S. and Poole, D. E. The compressible flow discharge coefficients for a two-dimensional slit. *Int. J. Mech. Sci.*, 1965, **7**, 337
20 Alder, G. M. The numerical solution of choked and supercritical ideal gas flow through orifices and convergent conical nozzles. *J.Mech. Eng. Sci.*, 1979, **21**, 197
21 Guitton, D. E. and Newman, G. B. Self-preserving turbulent wall jets over convex surfaces. *J. Fluid Mech.*, 1977, **81**, 155
22 Gilchrist, A. R. and Gregory-Smith, D. G. The compressible Coanda Wall Jet—predictions of jet structure and comparison with experiments. (to be published)

Book reviews

Technical Guide to Thermal Processes

J. Gosse

At the price of £7.95 the book, the work of a French professor of energy engineering, is good value. This compact volume of some 220 pages is, according to the publishers, intended as a course text for engineering students and a reference for professional engineers.

The subject area covered by book is described as thermal physics which basically consists of principles of thermodynamics, fundamental ideas and experimental data on the properties of fluids, heat transfer by conduction, convection and radiation and mass transfer. Because of the limited space available for the wide range of topics covered in the book, the treatment of the subject matter has necessarily to be concise. However, the concepts and principles of thermodynamic analysis, particularly different aspects of the Second Law, irreversibility and exergy analysis are not amenable to such a concise treatment and hence in this particular area the book is less than successful. Consequently, it cannot be recommended as a course text for engineering students. The book is much more successful where principles and laws of thermodynamics and heat transfer are expressible in a mathematical form. The equations relating to the different modes of heat transfer and mass transfer are numerous and up to date. These equations as well as those expressing laws of conservation of mass, energy and momentum have been stated in concise mathematical forms using, where applicable, vector and tensor notation. The book contains many useful tables and charts with thermo-chemical data, properties of substances and mathematical constraints. The general tenor of the book is academic rather than practical and therefore it will suit better research engineers and research students rather than practising professional engineers.

T. J. Kotas
Department of Mechanical Engineering,
Queen Mary College,
London, UK

Published price £22.50, by Cambridge University Press, The Edinburgh Building, Shaftesbury Road, Cambridge CBS 2RU, UK, 227 pp.